



GPS satellite differential code bias estimation with current eleven low earth orbit satellites

Xingxing Li¹ · Wei Zhang¹ · Keke Zhang¹ · Qian Zhang¹ · Xin Li¹ · Zihao Jiang¹ · Xiaodong Ren¹ · Yongqiang Yuan¹

Received: 25 October 2019 / Accepted: 13 June 2021 / Published online: 22 June 2021
© Springer-Verlag GmbH Germany, part of Springer Nature 2021

Abstract

Many low earth orbit (LEO) missions have been launched recently for different geoscience studying purposes such as ionosphere detecting and gravity recovering. The onboard observations from LEO satellites provide us a great opportunity to estimate the differential code bias (DCB) which is vital for precise applications of global navigation satellites system. This paper mainly focuses on the contribution of multi-LEO combination to the DCB estimation using onboard data collected by current eleven LEO satellites from day of year (DOY) 061, 2018 to DOY 120, 2018. The single-LEO solutions with different LEO and multi-LEO solutions with different LEO subsets are compared and analyzed in detail to fully exploit the potential of LEO onboard observations in the DCB estimation. We also evaluate and discuss the vertical total electron content (VTEC) results and posterior residuals to validate the estimation accuracy. Our results show that the average DCB standard deviation (STD) values are within 0.140 ns for all eleven single-LEO solutions with the best stability of 0.082 ns for Swarm-B solution. The evaluation of multi-LEO solutions indicates that with the increase in LEO satellites, the GPS DCB stability gets improved gradually. The 9-LEO solution can achieve the stability with STD value of 0.051 ns, better than that of DCB products from the German Aerospace Center (DLR) (0.055 ns) but slightly worse than that of DCB products from the Chinese Academy of Sciences (CAS) (0.048 ns). The results suggest that the GPS DCB stability based on the onboard observations of nine LEO satellites can be comparable to the ground-based solution derived from a global ground network with hundreds of stations. The LEO space-borne receiver DCB results illustrate that the inclusion of more LEO satellites can contribute to the stability improvement of receiver DCB. In addition, the VTEC estimation can benefit from the joint processing of multiple LEO observations and achieves a noticeable reduction in the percentage of negative VTEC values. Our results also reveal that the spherical symmetry ionosphere assumption might cause accuracy degradation in the DCB estimation at low latitudes.

Keywords Differential code bias (DCB) · Low earth orbit (LEO) onboard observations · Multi-LEO combination · Vertical total electron content (VTEC) · Spherical symmetry ionosphere assumption

1 Introduction

The differential code bias (DCB) is generally recognized as a kind of signal timing bias existing between two different types of code observations on the same or different frequencies. Since the DCB can significantly affect the accuracy of total electron content (TEC) estimation, the precise knowledge of DCB values is required in the ionosphere modeling (Schaer 1999; Hernández-Pajares et al. 1999). In addition,

as one of the major error sources for GNSS observations, the DCB must be considered in precise applications of global navigation satellite system (GNSS), such as precise point positioning (PPP) (Li et al. 2018a; Ge et al. 2017) and satellite clock estimation (Li et al. 2016) owing to the use of code observations.

Recently, many low earth orbit (LEO) missions have been launched for different geoscience studying purposes, such as Swarm for ionosphere detecting (Friis-Christensen et al. 2008), Sentinel for ocean surveying (Aschbacher and Milagro-Pérez 2012), the Meteorological Operational satellite (MetOp) for meteorology monitoring (Edwards et al. 2006), and the Gravity Recovery and Climate Experiment (GRACE) for gravity recovering (Tapley et al. 2004). The

✉ Keke Zhang
kkzhang@whu.edu.cn

¹ School of Geodesy and Geomatics, Wuhan University, 129 Luoyu Road, Wuhan 430079, China

precise science orbit of LEO satellites is a key issue to fulfill the scientific objectives of these missions. In the precise orbit determination (POD) of LEO satellites, the DCB can significantly affect the orbit accuracy and should be calibrated. Despite the fact that DCB values of GPS satellites have been calibrated before launch, they still suffer from distortion caused by many factors, such as hardware aging, and space temperature (Sanz et al. 2017). It is, therefore, of vital importance to determine the DCB during the period of GPS satellite in orbit.

Aiming to provide high-accuracy DCB and ionospheric vertical total electron content (VTEC) products, the international GNSS service (IGS) started the ionospheric working group in June 1998 (Feltens 2003; Hernández-Pajares et al. 2009). Generally, there are two main methods to estimate the DCB (Li et al. 2014; Wang et al. 2015). The first one is estimating the ionosphere model and DCB values simultaneously (Mannucci et al. 1998; Hernández-Pajares et al. 1999). A well-known application of this approach is the generation of Global Ionospheric Maps (GIMs). Apart from this approach of DCB estimation, another method is eliminating the ionosphere delay with a priori ionospheric model before the estimation. The DCB products provided by the German Aerospace Center (DLR) were generated by utilizing the GIMs to eliminate the slant total electron content (STEC) parameters (Montenbruck et al. 2014). Also, Li et al. (2018b) estimated the DCBs for Chinese BeiDou satellite system (BDS-2 and BDS-3) using this approach.

Currently, all DCB products are generated from GNSS observations of ground stations. The DCB precision of the ground-based DCB estimation is mainly within 0.05–0.30 ns in terms of the day-to-day repeatability for most DCB products provided by analysis centers (ACs), such as the Center of Orbit Determination in Europe (CODE) and the Chinese Academy of Science (CAS) (Montenbruck et al. 2014; Wang et al. 2015). Although the ground-based DCB products have shown valuable GNSS applications, the drawbacks still exist in two aspects. On the one hand, the ground stations are mainly distributed in continental regions while ocean regions are hardly covered. The distribution of ground stations would affect the accuracy of satellite DCB estimates (Wang et al. 2015). On the other hand, the observations from ground stations suffer from severe ionosphere errors due to the ionospheric ionization especially in the ionosphere area of high electron density such as F layer. The observation errors caused by the ionosphere will be mapped into the DCB parameters, thus leading to the severe degradation of DCB accuracy (Yue et al. 2011; Noja et al. 2013).

Since most LEO satellites of geodetic missions have been equipped with dual-frequency space-borne receivers, the approach of estimating DCB by utilizing the LEO onboard data was proposed. Different from ground stations, the ground tracks of LEO satellites can cover most regions

without being restricted by the ground environment. In addition, most LEO satellites orbit at the altitude of topside ionosphere. Due to the low electron density of topside ionosphere, the LEO-based DCB estimation can be less affected by the ionospheric ionization (Hernández-Pajares et al. 2011; Zhong et al. 2016a). Three methods have been widely applied in the LEO-based DCB estimation. The first method is under the assumption that the ionosphere model is as accurate as the real ionospheric electron density. Hence, the LEO receiver DCB can be calculated by subtracting the modeled TEC value from the measured TEC value (Heise et al. 2002). However, this method has a strong dependence on the accuracy of the ionosphere model. The second one adopted by Lee et al. (2013) assumed that the measured TEC above the LEO satellite is close to zero in the area of high latitudes or during nighttime. This method can be easily affected by observation errors such as cycle slip and multipath errors. The third method is the application of the spherical symmetry assumption under which the VTEC is identical for different GPS satellites at the same epoch (Yue et al. 2011; Zakharenkova and Cherniak 2015; Wautelet et al. 2017; Li et al. 2019a). The VTEC parameters are estimated along with DCB. This method can work well in most cases but might cause accuracy degradation in the DCB estimation at low latitudes (Yue et al. 2010). Based on three methods above, the existing literature has proved the great potential of LEO-based DCB estimation. Nevertheless, the majority of previous studies are based on the onboard observations from single LEO satellite. The advantage of onboard observations for the DCB estimation has not been fully exploited. Thanks to the availability of onboard data from so many LEO satellites, we get a great opportunity to investigate the contribution of multi-LEO combination to the DCB estimation. Considering the limited accuracy of the current plasmasphere model (Zhang and Tang 2014) and the different observation error-level for LEO satellites, we adopted the spherical symmetry assumption which has been widely applied in the DCB estimation.

In this paper, we mainly focus on the contribution of multi-LEO onboard observations to the DCB estimation. The paper is organized as follows: In Sect. 2, the method and strategy utilized in the DCB computation are presented. In Sect. 3, the corresponding results are displayed and discussed which consists of four parts: In Sect. 3.1, the multipath errors for each LEO satellite are analyzed. The contribution of observations from single LEO satellite and multiple LEO satellites to the DCB estimation is assessed in the Sect. 3.2 and Sect. 3.3, respectively. In Sect. 3.4, the impact of multi-LEO combination on VTEC results is evaluated. The posterior residual results for different LEO satellites are analyzed in Sect. 3.5. In Sect. 3.6, we made a discussion of the advantages and disadvantages of the LEO-based method and the ground-based method in the

DCB estimation. In Sect. 4, the summary and conclusions are given.

2 DCB estimation method and strategy

The onboard dual-frequency observations of the pseudorange and carrier phase can be expressed as follows:

$$\begin{cases} P_{r,i}^s = \rho_r^s + \frac{40.3}{f_i^2} \cdot \text{STEC}_r^s + c \cdot (dt_r - dt^s) + b_{r,i} + b^{s,i} + \text{MP}_{r,i} + \xi_i \\ L_{r,i}^s = \rho_r^s - \frac{40.3}{f_i^2} \cdot \text{STEC}_r^s + c \cdot (dt_r - dt^s) + B_{r,i}^s + \Delta \varphi_{r,i}^s + \varepsilon_i \end{cases} \quad (1)$$

where $P_{r,i}^s$ and $L_{r,i}^s$ represent the pseudorange and carrier phase observations, respectively. The superscript s denotes the GPS satellite. The subscript r and i represent the onboard receiver and the frequency, respectively. ρ refers to the geometric distance between the GPS satellite and the LEO onboard receiver. f is the frequency. STEC represents the slant total electron content in the unit of TECU. c is the light speed in vacuum. dt_r and dt^s denote the clock offsets of the LEO onboard receiver and the GPS satellite, respectively. $b_{r,i}$ and $b^{s,i}$ represent the instrument delay of the LEO onboard receiver and the GPS satellite, respectively. $B_{r,i}^s$ is the float ambiguity in the unit of meter. $\Delta \varphi_{r,i}^s$ denotes the phase wind-up error. $\text{MP}_{r,i}$ represents the multipath error of pseudorange. ξ_i and ε_i refer to as the measurement noise of the pseudorange and carrier phase observations, respectively.

Based on Eq. (1), the geometry-free combination of the pseudorange and carrier phase observations can be formed as follows:

$$\begin{cases} P_{r,12}^s = P_{r,1}^s - P_{r,2}^s = \alpha \cdot \text{STEC} + \text{DCB}_r + \text{DCB}^s + \Delta \text{MP}_{r,12} + \Delta \xi_{12} \\ L_{r,12}^s = L_{r,1}^s - L_{r,2}^s = -\alpha \cdot \text{STEC} + B_{r,12}^s + \Delta \varphi_{r,12} + \Delta \varepsilon_{12} \end{cases} \quad (2)$$

where $P_{r,12}^s$ and $L_{r,12}^s$ denote the geometry-free combination of the pseudorange and carrier phase observations, respectively. $\alpha = 40.3 \cdot \frac{f_2^2 - f_1^2}{f_1^2 f_2^2}$ is the combination coefficient of STEC. DCB_r and DCB^s represent the differential code biases of the LEO onboard receiver and the GPS satellite, respectively. $B_{r,12}^s = B_{r,1}^s - B_{r,2}^s$ is the combined phase ambiguity. $\Delta \text{MP}_{r,12}$ and $\Delta \varphi_{r,12}$ refer to as the difference of multipath error of pseudorange and phase wind-up error on two frequencies. $\Delta \xi_{12}$ and $\Delta \varepsilon_{12}$ represent the measurement noise differences of the pseudorange and the carrier phase, respectively. It should be noted that the multipath error of pseudorange and the phase wind-up error cannot be ignored and should be eliminated when using LEO onboard data to compute the DCB (Yue et al. 2011; Li et al. 2017).

According to Eq. (2), the ionosphere delay can be removed by combining $P_{r,12}^s$ and $L_{r,12}^s$. After the calibration of the multipath and the phase wind-up errors, the corresponding result can be expressed as follows:

$$L_{sm} = P_{r,12}^s + L_{r,12}^s = \text{DCB}_r + \text{DCB}^s + B_{r,12}^s + \Delta \xi_{12} \quad (3)$$

Since the DCBs of the LEO onboard receiver and the GPS satellite are rather stable in one continuous arc and the phase ambiguities would not change when no cycle slips occur, L_{sm} can be averaged in one continuous arc which can significantly reduce the noise of pseudorange (Yue et al. 2011):

$$\hat{L}_{sm} = \frac{\sum_{n=1}^N L_{sm}}{N} = \text{DCB}_r + \text{DCB}^s + B_{r,12}^s \quad (4)$$

where N is the number of epochs of one continuous arc. By combining Eq. (3) and Eq. (4), we have:

$$\hat{P}_{r,12} = \hat{L}_{sm} - L_{r,12}^s = \alpha \cdot \text{STEC} + \text{DCB}_r + \text{DCB}^s \quad (5)$$

where $\hat{P}_{r,12}$ represents the carrier phase smoothed pseudorange observation. According to Eq. (5), a rank deficiency will occur when STEC along the receiver-to-satellite path is estimated as an independent parameter per epoch. In order to eliminate this deficiency, we employ the spherical symmetry assumption proposed by Yue et al. (2011). Under this assumption, the VTEC is identical for different GPS satellites at the same epoch. The relationship between VTEC and STEC can be expressed as:

$$\text{STEC} = mf \cdot \text{VTEC} \quad (6)$$

where mf denotes the mapping function. The existing studies report that the F&K mapping function can work well in the LEO-based DCB estimation (Foelsche and Kirchengast 2002; Zhong et al. 2016b; Yue et al. 2011; Lin et al. 2014). The F&K mapping function is expressed as:

$$mf = \frac{1 + (H_{\text{hell}} + R_e)/(H_{\text{LEO}} + R_e)}{\cos z + \sqrt{(H_{\text{shell}} + R_e)^2/(H_{\text{LEO}} + R_e)^2 - \sin^2 z}} \quad (7)$$

where R_e refers to the earth radius. H_{LEO} represents the orbit altitude of LEO satellite. z refers to the elevation angle from the LEO onboard receiver to the GPS satellite. H_{shell} denotes the ionosphere effective height (IEH). Herein, the IEH is set to 2000 km as performed by Wautelet et al. (2017).

Assuming that the number of LEO satellites is n and m GPS satellites are available for every LEO satellite, the equation of the observation model for a given epoch can be formed as Eq. (8), where \hat{P}_i^j denotes the carrier phase smoothed pseudorange observation between LEO $_i$ and GPS $_j$. mf_i^j represents the mapping function w.r.t. LEO $_i$ and GPS $_j$. VTEC_i , DCB_i , DCB^j refer to as the VTEC parameter of

LEO_{*i*}, the receiver DCB parameter of LEO_{*i*}, and the satellite DCB parameter of GPS_{*j*}, respectively. For each LEO satellite, the same VTEC is estimated at a given epoch for all GPS satellites owing to the use of the spherical symmetry ionosphere assumption, while the DCB parameter of each LEO/GPS satellite is estimated as a constant for one day owing to the stable characteristic of the DCB. Since the GPS satellite DCB parameters and the onboard receiver DCB parameters are closely coupled and cannot be separated, the “zero-constellation-mean” constraint is adopted in this study to eliminate the rank-defect (Montenbruck et al. 2014). Herein we assume that the sum of all GPS satellite DCBs is equal to zero. In the estimation, the least-squares method is adopted.

$$\begin{pmatrix} \hat{P}_1^1 \\ \hat{P}_1^2 \\ \vdots \\ \hat{P}_1^m \\ \hat{P}_2^1 \\ \vdots \\ \hat{P}_n^1 \\ \vdots \\ \hat{P}_n^m \end{pmatrix} = \begin{pmatrix} \alpha \cdot mf_1^1 & 0 & \dots & 0 & 1 & \dots & 0 & 1 & \dots & 0 \\ \alpha \cdot mf_1^2 & 0 & \dots & 0 & 1 & \dots & 0 & 0 & \dots & 0 \\ \vdots & \vdots & \vdots & \vdots & \vdots & \vdots & \vdots & \vdots & \vdots & \vdots \\ \alpha \cdot mf_1^m & 0 & \dots & 0 & 1 & \dots & 0 & 0 & \dots & 1 \\ 0 & \alpha \cdot mf_2^1 & \dots & 0 & 0 & \dots & 0 & 1 & \dots & 0 \\ \vdots & \vdots & \vdots & \vdots & \vdots & \vdots & \vdots & \vdots & \vdots & \vdots \\ 0 & \alpha \cdot mf_n^1 & \dots & 0 & 0 & \dots & 0 & 1 & \dots & 0 \\ \vdots & \vdots & \vdots & \vdots & \vdots & \vdots & \vdots & \vdots & \vdots & \vdots \\ 0 & 0 & \dots & \alpha \cdot mf_n^m & 0 & \dots & 1 & 0 & \dots & 1 \end{pmatrix} \begin{pmatrix} \text{VTEC}_1 \\ \text{VTEC}_2 \\ \vdots \\ \text{VTEC}_n \\ \text{DCB}_1 \\ \vdots \\ \text{DCB}_n \\ \text{DCB}^1 \\ \vdots \\ \text{DCB}^m \end{pmatrix} \tag{8}$$

Eleven LEO satellites with different orbit height and inclination, which include MetOp-A, MetOp-B, Sentinel-1A, Sentinel-1B, Sentinel-2A, Sentinel-2B, Sentinel-3A, Swarm-A, Swarm-B, Swarm-C, and TerraSAR-X have been selected. The detailed information about each LEO satellite are listed in Table 1. Note that the onboard receivers of the LEO satellites from the same mission

are identical. The existing study reports that the Sentinel receivers closely match the receivers mounted on Swarm satellites (Montenbruck et al. 2018). Since most selected LEO satellites orbit the earth in sun-synchronous orbits, the local equator crossing time is also given in the table. LEO onboard observations during the period from the day of year (DOY) 061, 2018 to DOY 120, 2018 are utilized to estimate the GPS DCB values. The interval is set to 60 s, and the cutoff elevation mask is 30°. An elevation-dependent weighting strategy is applied for the DCB estimation. For the sake of removing the outlier and cycle slip of carrier phase, the TurboEdit algorithm proposed by Blewitt (1990) was adopted in this study. Considering the observation types for all LEO satellites, only P2-C1 differential code bias is estimated.

With the adoption of the method and strategy above, we aim to fully exploit the potential of multi-LEO combination in the DCB estimation and provide an effective alternative approach of DCB estimation only using LEO onboard data. The data quality control processing, such as the cycle slip detection and the multipath error correction, has been performed before the estimation. Both single-LEO solutions and multi-LEO solutions are compared and analyzed to investigate the contribution of multi-LEO combination to the DCB estimation. The results are evaluated in terms of the GPS DCB (stability and comparison with DLR/CAS DCB products), the LEO space-borne receiver DCB (stability and comparison with external DCB products), and the VTEC (percentage of negative VTEC and comparison with external VTEC products). In addition, we also assessed the posterior residuals to validate the DCB estimation accuracy and discussed the impact of the spherical symmetry assumption on the LEO-based DCB estimation.

Table 1 Information of all eleven LEO satellites in the DCB estimation

LEO Satellite	Altitude/km	Inclination/deg	Receiver type	Antenna type	Orbit type	A/DLECT
MetOp-A	817	98.74	GRAS	PA	S-S	21:30/9:30
MetOp-B	817	98.74	GRAS	PA	S-S	21:30/9:30
Sentinel-3A	814	98.65	GPSR	PEC+CR	S-S	22:00/10:00
Sentinel-2A	786	98.82	GPSR	PEC+CR	S-S	22:30/10:30
Sentinel-2B	786	98.82	GPSR	PEC+CR	S-S	22:30/10:30
Sentinel-1A	693	98.18	GPSR	PEC+CR	S-S	6:00/18:00
Sentinel-1B	693	98.18	GPSR	PEC+CR	S-S	6:00/18:00
TerraSAR-X	514	97.44	IGOR	PA+CR	S-S	18:00/6:00
Swarm-B	511	87.35	GPSR	PEC	DO	–
Swarm-A	462	87.35	GPSR	PEC	DO	–
Swarm-C	462	87.35	GPSR	PEC	DO	–

GRAS, GNSS Receiver for Atmospheric Sounding; GPSR, GPS Receiver; IGOR, Integrated GPS and Occultation Receiver; PEC, Patch Excited Cup; PA, Patch Antenna; CR, Choke Ring; S–S, Sun-Synchronous; DO, Drifting Orbit; A/DLECT, Ascending/Descending Local Equator Crossing Time

3 Results and discussion

3.1 Analysis of LEO satellite multipath errors

Because of the deflection of GPS signals caused by solar panels and the cross-talk between different antennas (e.g., navigation antenna and occultation antenna), the multipath errors of LEO code observations are worse-than-expected (Li et al 2017; Hwang et al. 2010; Yue et al. 2011). Hence, the multipath errors of code observations for each LEO satellite are calculated using multipath combination proposed by Montenbruck and Kroes (2003) before the DCB estimation. Here, the multipath error is expressed as a function of elevation and azimuth in the LEO antenna reference frame (ARF). The antenna reference frame is defined as follows: The origin is located at the mechanical antenna reference point (ARP) which is given in the satellite-fixed coordinate system, with the $+x$ axis pointing along the flying direction and the $+z$ axis pointing along the boresight direction, while the y axis completes a left-hand coordinate system (Jäggi et al. 2009). The azimuth is counted from the $+x$ axis in a clockwise direction.

As shown in Fig. 1, the CA code observations of Swarm and Sentinel satellites present a low multipath error level in most areas and the overall magnitude of the multipath errors is within 0.2 m. This can be due to the equipment

of PEC-elements antennas which have special features to minimize their coupling to the surrounding spacecraft environment for these LEO satellites (Gao et al. 2009; Öhgren et al. 2011). The multipath errors in the fore hemisphere are larger than those of hind hemisphere, especially at low elevation, which is more noticeable for Swarm satellites. This is reasonable because compared with Swarm antennas, Sentinel antennas have been equipped with two choke rings which can mitigate the multipath errors (Öhgren et al. 2011). However, different from Swarm and Sentinel satellites, the onboard observations of MetOp satellites suffer from much severe multipath errors. It can be attributed to the fact that these satellites have been equipped with patch antennas (Montenbruck et al. 2008, 2009) which may bring about severe multipath errors owing to the relatively poor polarization purity and narrow bandwidth (Hwang et al. 2010; Montenbruck and Kroes 2003; Bankey and Anvesh Kumar 2015). The multipath errors of MetOp satellites can reach up to 0.4 m, which are nearly symmetrically distributed along the y axis but has opposite signs. Thanks to the equipment of choke rings, the multipath errors of TerraSAR-X satellite are smaller than those of MetOp satellites except for the areas at low elevation. In addition, we can find that the LEO satellites which carry an identical space-borne receiver present a similar multipath error pattern.

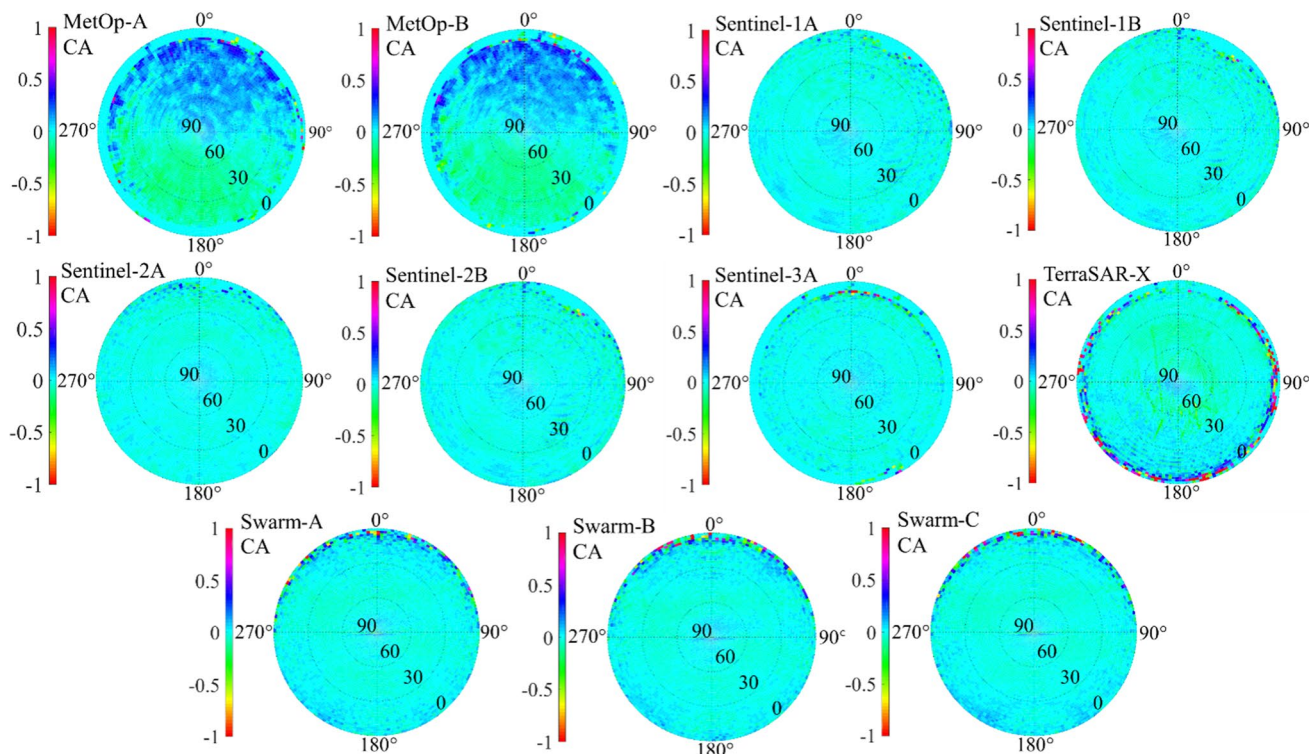


Fig. 1 Distribution and magnitude of CA code multipath errors with grid solution of $2^\circ \times 2^\circ$ for individual LEO satellite (Unit: m)

Based on the multipath error results above, significant differences can be noted in the magnitude and the distribution of multipath errors between different LEO missions. The traditional approach of multipath elimination used for ground stations by discarding low elevation observations, therefore, is not applicable for LEO satellites (Yue et al. 2011), especially for MetOp satellites, which exhibit much larger multipath errors even at high elevation. Hence, in order to eliminate the negative impact of multipath errors on the DCB estimation, the multipath errors of each LEO satellite have been corrected according to the calculated multipath map below.

3.2 DCB estimation results with single LEO satellite

In this section, we perform the DCB estimation of GPS satellites using only single LEO onboard observations. All data from aforementioned LEO satellites are processed separately. The DCB results are evaluated from the following two aspects: (1) The standard deviation (STD) values of the daily DCBs. (2) Comparison with the GPS DCB products from DLR and CAS.

Figure 2 displays the DCB STD values of individual GPS satellites for all single-LEO solutions. WHU refers to our DCB estimation results. The STD values of DCB products from DLR and CAS are also computed for comparison. It can be seen that the LEO-based DCB solutions present larger STD values than those of the DLR and CAS products.

This is mainly because DLR/CAS products are estimated by ground observations from hundreds of global sites, whereas the WHU solution only uses the observations from a single LEO satellite to estimate the differential code biases. The DCB STD values of most GPS satellites for all single-LEO solutions are below 0.14 ns. Among all solutions, the best stability of the estimated DCB can be found for the Swarm-B solution with an average STD value of about 0.082 ns. By comparison, the DCB of the MetOp-A/B solution shows a slightly larger STD value. The slightly poorer performance of the MetOp-A/B solution can be attributed to the poor code observations with more noise after MP correction as shown in Fig. 3. In the DCB estimation, more available observations with good quality can bring an increase in the observation redundancy, which will yield a rise in the strength of DCB estimation, especially when only single-LEO observations are used. Our estimation is also in accord with a previous study by Wautelet et al. (2017) and exhibits a slightly better performance in terms of some LEO satellites such as Swarm-A/B/C. It implies that our single-LEO solution can offer stability comparable to that of solution relying on tens of ground stations. In addition, no significant correlation can be observed between the LEO orbit altitude and the DCB stability. Since the observation quality and number are correlated with the receiver performance, the LEO satellites which carry an identical space-borne receiver present a similar DCB result, such as Swarm-A, B, and C (Fig. 4).

Fig. 2 DCB STD values of each GPS satellite for all single-LEO solutions. The red, cyan, and blue bars represent the estimated results (WHU), the products from DLR and CAS, respectively

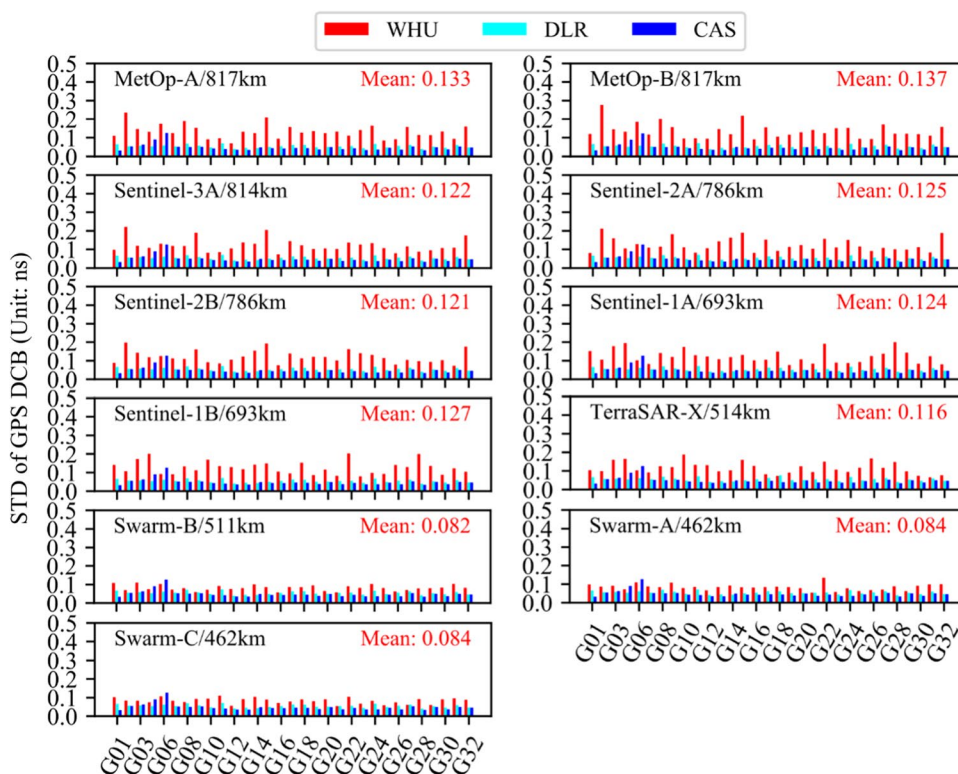


Fig. 3 Code noise with respect to the elevation angle for each LEO satellite with cut-off elevation of 30° after MP correction

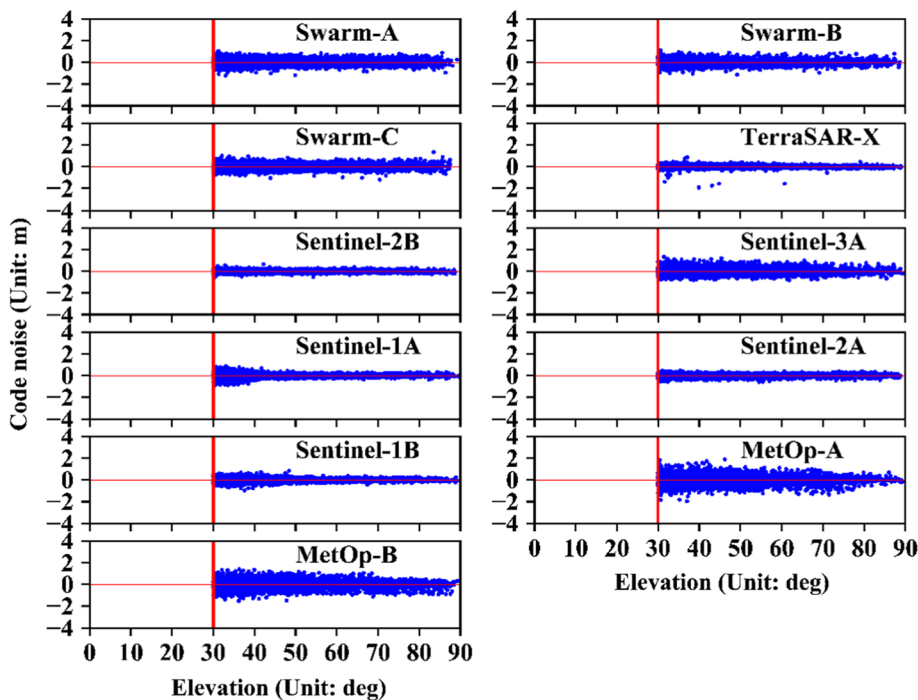


Fig. 4 Average number of available observations for each LEO satellite

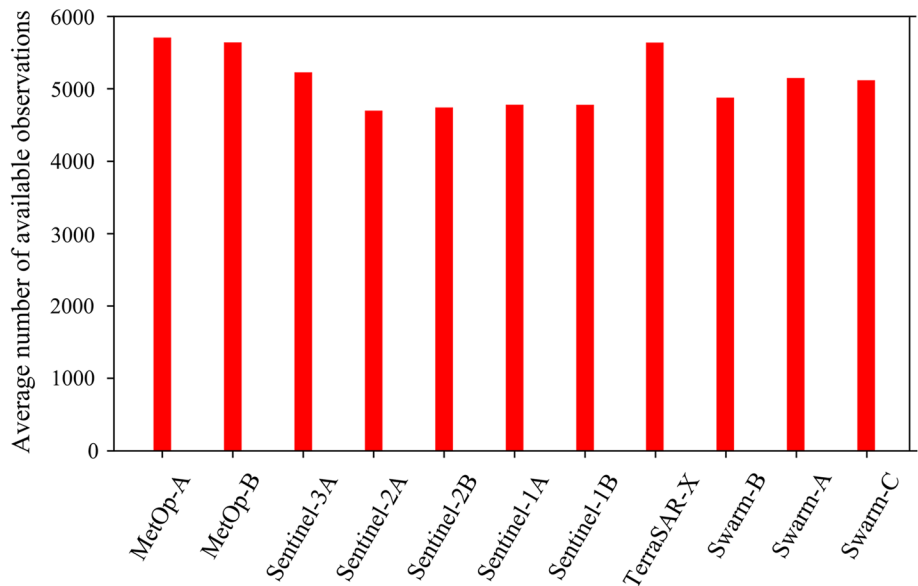


Figure 5 shows the mean DCB differences between the WHU solution and DLR/CAS products of each GPS satellite. The mean DCB differences exhibit a variation ranging from -0.5 ns to 0.5 ns for most GPS satellites. Similar results can also be found in the previous literature by Li et al. (2019a, b) and Wautelet et al. (2017) which studied the DCB estimation based on single LEO satellite. Meanwhile, Fig. 6 displays the mean and STD values of DCB differences of the GPS constellation. The results of the TerraSAR-X solution exhibit the best consistency with the DCB products from DLR/CAS with mean and STD

values of 0.219 ns and 0.021 ns for WHU-DLR, 0.223 ns and 0.001 ns for WHU-CAS, respectively. This superior performance might be associated with the large number of available observations of TerraSAR-X satellite (see Fig. 4). Despite the similar numbers of available observations from TerraSAR-X and MetOp satellites, mean values for MetOp-A/B solution are much larger than those of TerraSAR-X solution. This is mainly because compared to the IGOR receiver on TerraSAR-X satellite, the GRAS instrument exhibits much larger pseudorange noise as indicated from Fig. 3 owing to its more conservative loop

Fig. 5 Mean DCB differences between the WHU solution and DLR/CAS products of individual GPS satellite for all single-LEO solutions

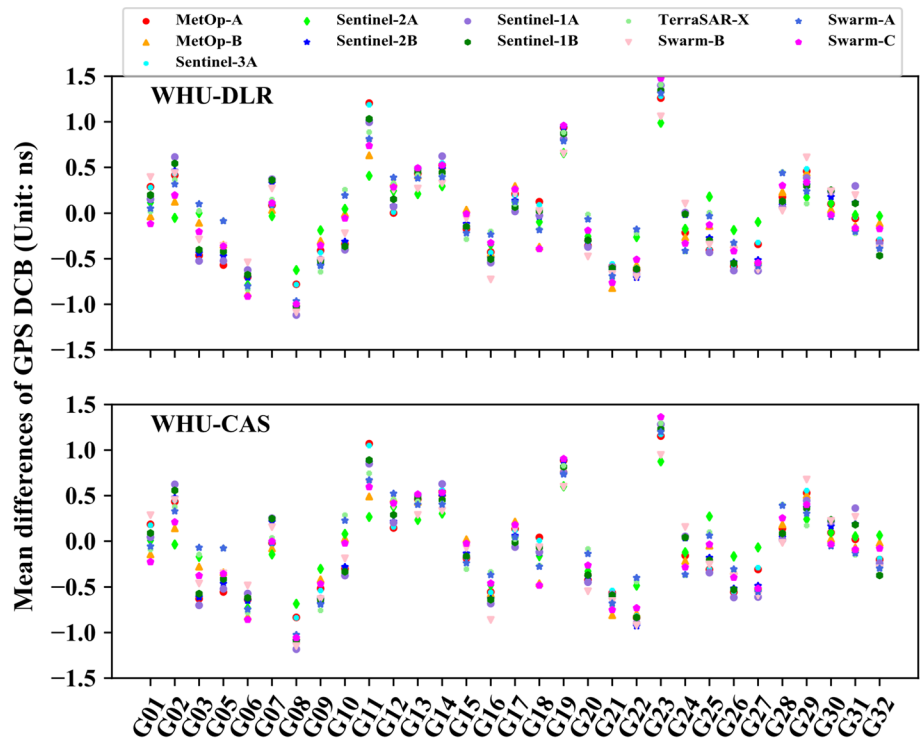
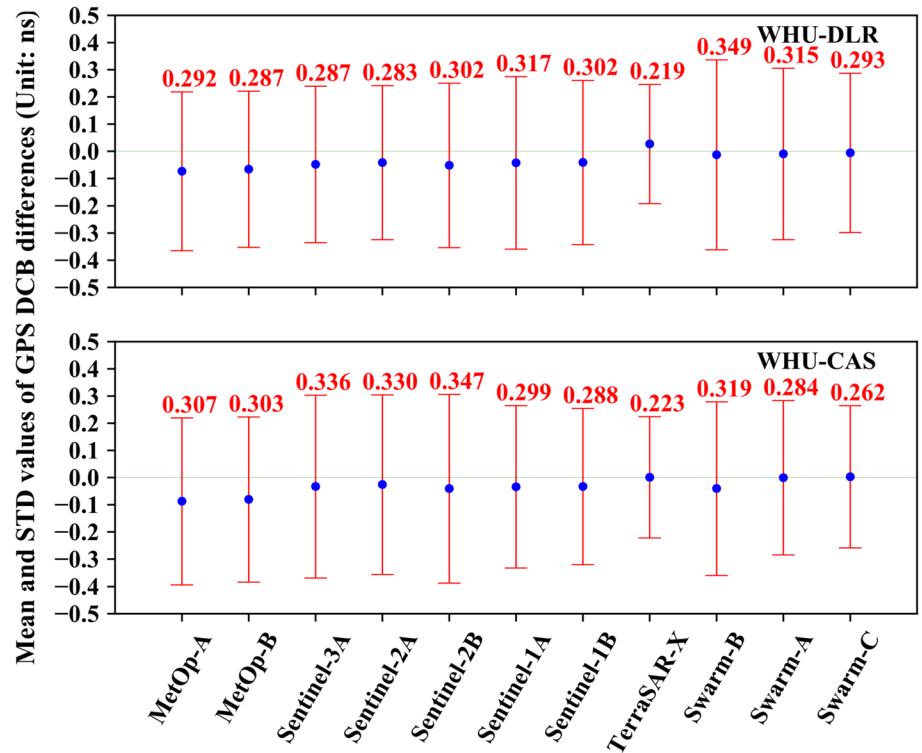


Fig. 6 Mean and STD values of DCB differences of the GPS constellation for all single-LEO solutions. The blue dot represents the mean difference, and the red error bar represents the STD value

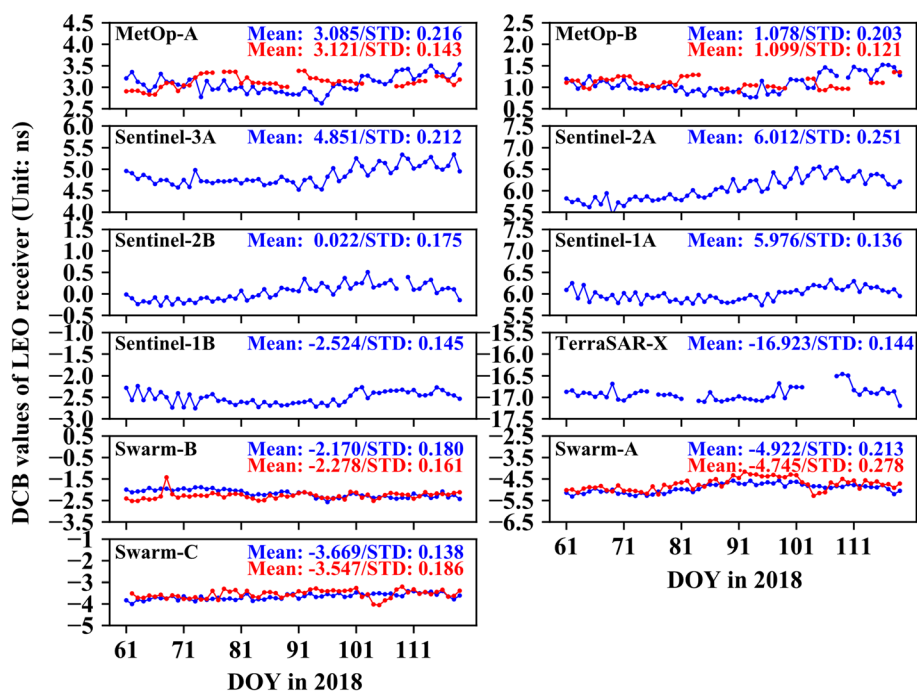


settings and the lack of a choke ring (Montenbruck et al. 2008), thus leading to the poorer quality of observations.

The receiver DCBs of LEO satellites are displayed in Fig. 7. To evaluate our DCB results, the DCB products

of MetOp satellites from CDAAC and DCB products of Swarm satellites from GFZ are also displayed as external reference. Note that the time series of calculated receiver DCBs for TerraSAR-X satellite and the DCB

Fig. 7 DCB values of LEO onboard receiver for all single-LEO solutions. The mean and STD values of the receiver DCBs are displayed on the upper right corner of each panel. The red line represents the DCB products from analysis centers



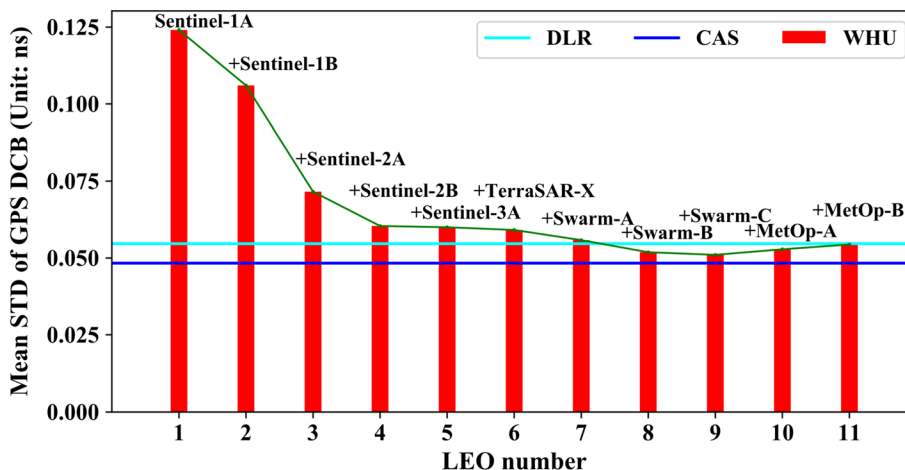
products of MetOp satellites are discontinuous on some days owing to missing data. As shown in Fig. 7, there are obvious differences between the receiver DCB values of these LEO satellites. The maximum DCB mean values of 5.976 ns can be observed for Sentinel-1A satellite, while TerraSAR-X satellite shows the minimum mean value of -16.923 ns. In terms of the stability of receiver DCBs, STD values of onboard receivers for all LEO satellites are within 0.26 ns. The receiver DCBs of Sentinel-1A and Swarm-C show the best stability which can reach 0.14 ns. Compared with the results of GPS DCBs, the DCBs of LEO satellites exhibit a larger variation. Considering the shorter revolution period and eclipses of LEO satellites, the environment of onboard receiver, such as temperature, changes a lot quickly which can significantly affect the hardware thermal status (Zhong et al. 2016c). Hence, the LEO satellite DCBs show a more noticeable instability than those of GPS satellites. The obvious receiver DCB differences between different LEO satellites can be attributed to the dissimilarity of the receiver environment as well as the receiver performance for different LEO satellites. The comparison results between our estimated receiver DCB and the external DCB products indicate that our estimation agrees well with the MetOp DCB products and Swarm DCB products. Moreover, in terms of the STD values of receiver DCB, our estimates of MetOp receiver DCB exhibit better stability than the MetOp DCB products.

3.3 DCB estimation results with multiple LEO satellites

In this section, onboard observations from multiple LEO satellites are processed to estimate the differential code biases of GPS satellites. In order to assess the impact of the number of LEO satellites on the DCB estimation, ten combination solutions of multiple LEO satellites have been designed and the corresponding LEO numbers vary from two to eleven. Given the numerous combinations of multiple LEO satellites, we just present the DCB results of one combination of LEO satellites for each multi-LEO solution. The Sentinel-1A solution is chosen as the 1-LEO solution. Then we add one LEO satellite to the DCB estimation process each time as a new multi-LEO solution. The added LEO satellites in turn are Sentinel-1B, Sentinel-2A, Sentinel-2B, Sentinel-3A, TerraSAR-X, Swarm-A, Swarm-B, and Swarm-C, respectively.

We have calculated the mean STD values of each solution and the corresponding results are depicted in Fig. 8. It shows that the GPS DCB stability improves gradually with increasing number of LEO satellites. In comparison with the result of the 1-LEO solution, the GPS DCB STD gets an evident reduction of 14.5%, 41.9%, and 51.6% when the LEO number increases to two, three, and four, respectively. The improvement is the result of increase in available observations which can contribute a lot to reducing the uncertainty on the GPS DCBs. When the LEO satellite number reaches

Fig. 8 Mean STD values of GPS DCBs for all multi-LEO solutions. The red bar represents the mean DCB STD value of each multi-LEO solution. The cyan and blue lines represent the STD values of the DCB products from DLR and CAS, respectively. The green line shows the mean STD variation trend for all solutions



nine, the DCB STD is 0.051 ns, which is better than that of DLR with STD value of 0.055 ns and close to the result of CAS with STD value of 0.048 ns. The result suggests that only using the onboard observations from nine LEO satellites, the LEO-based solution can offer stability comparable to the ground-based solution which relies on a global network of hundreds of stations, even achieves a better performance. To further investigate the cause for the stability improvement of GPS satellite DCB, we have calculated the mean number of LEO satellites observed by each GPS satellite for all multi-LEO solutions as shown in Fig. 9. It can be found that the average LEO number increases gradually with the use of observations from more LEO satellites. It is worth noting that when the LEO number exceeds nine, the

GPS DCB stability even gets slightly worse. This is mainly because the introduction of low-quality observations from MetOp satellites taints the DCB estimation. The result demonstrates that the GPS DCB stability improves gradually with the use of more high-quality observations from LEO satellites.

The mean differences between the estimated DCB (WHU) results and CAS/DLR products for all multi-LEO solutions have been calculated as displayed in Fig. 10. The mean DCB differences for most GPS satellites exhibit dissimilarity with a variation ranging from -0.5 ns to 0.5 ns. This agrees with the results reported by Liu et al. (2020) which discussed the DCB estimation based on four LEO satellites. In comparison with the 1-LEO solution, the

Fig. 9 Average number of LEO satellite observed by each GPS satellite for all multi-LEO solutions

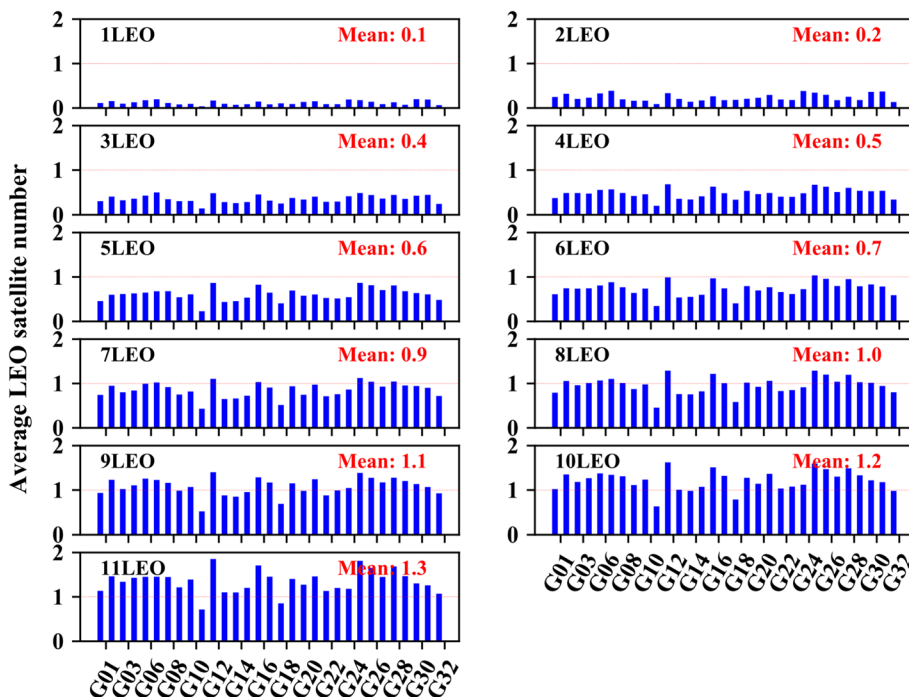


Fig. 10 Mean DCB differences of all GPS satellites for all multi-LEO solutions. The points with different colors refer to different solution. The DCB difference RMS values are given in the legend (left: WHU-DLR, right: WHU-CAS)

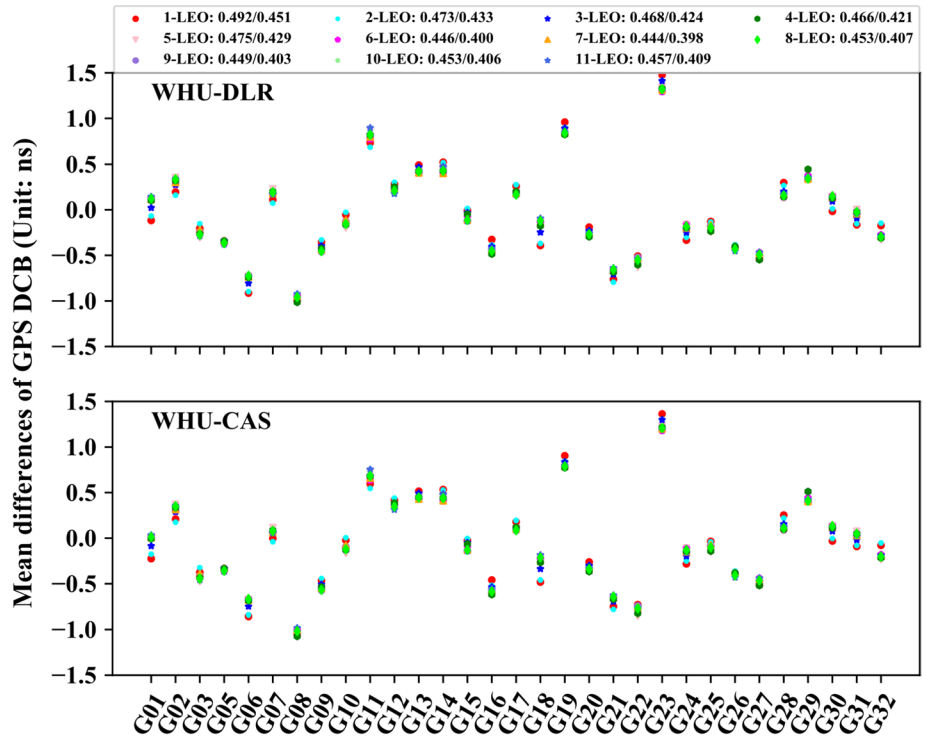
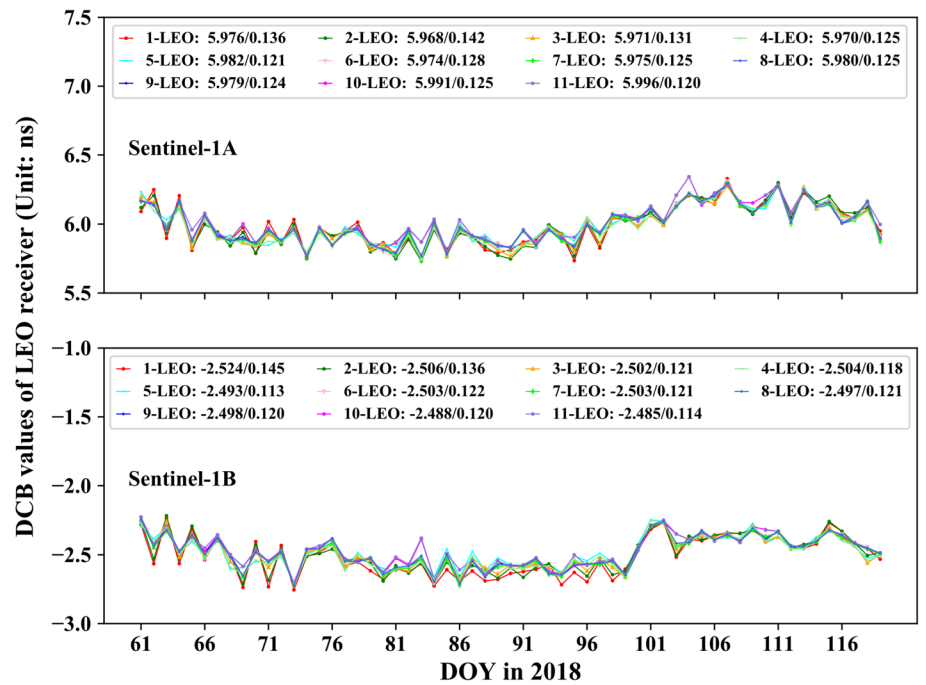


Fig. 11 DCB values of Sentinel-1A and Sentinel-1B receivers for all multi-LEO solutions. Different lines represent different multi-LEO solutions. For each solution, the mean and STD values of receiver DCB are shown in the top of each panel



root mean square (RMS) values of DCB differences for the 11-LEO solution get reduced by 7.1% and 9.3% for WHU-DLR and WHU-CAS, respectively. The comparison results of different solutions indicate that the increase in LEO satellites can contribute to the improvement of the consistency between our results and the external products.

The contribution of multi-LEO observations to the receiver DCB estimation is also evaluated. Figure 11 typically shows the time series of receiver DCBs for Sentinel-1A and Sentinel-1B satellites. For Sentinel-1A as well as Sentinel-1B satellite, the receiver DCB values have similar variation trends for all solutions. In comparison with the result

of the 1-LEO solution, the STD value of receiver DCBs gets reduced by 11.8% and 21.4%, and mean value gets slightly increased by 0.3% and 1.5% for Sentinel-1A and Sentinel-1B, respectively, when the LEO satellite number reaches eleven. The result above demonstrates that the multi-LEO combination can contribute to the stability improvement of receiver DCB.

3.4 Impact of multi-LEO combination on VTEC results

In our study, the VTECs of LEO satellites are estimated along with the GPS satellite and receiver DCBs. In general, the DCB estimation usually generates negative VTECs using LEO onboard observations (Wautelet et al. 2017). These negative values are the results of the underestimation of VTEC parameters and have no physical meaning (Li et al. 2017, 2019a). Due to low electron density of topside ionosphere, the VTECs derived from the DCB estimation using LEO satellite observations are usually small and even close to zero particularly for the LEO satellite with higher altitude. In that case, the generation of negative VTECs can be noticeable especially when the estimation strength is weak. Hence, the percentage of negative VTECs to all VTECs can reflect the degree of the VTEC underestimation, which can indirectly present the precision of the DCB estimation. In this section, the percentage of negative VTECs has been calculated in order to assess the impact of multi-LEO combination on the VTEC estimation.

Figure 12 shows the percentages of negative VTECs for all single-LEO solutions. We can find that the negative VTEC percentage of each LEO satellite varies a lot. The best VTEC estimation performance is achieved by Swarm-A satellite with a percentage of 1.3%, followed by Swarm-C

satellite with a percentage of 2.4%. By comparison, the negative VTEC percentage of Swarm-B satellite is much larger which can reach 10%. This can be attributed to the smaller topside ionosphere VTEC of Swarm-B which can easily become negative owing to the higher altitude. For LEO satellites at higher altitude such as Sentinel and MetOp, the generation of negative VTEC is more noticeable. Despite the lower altitude of TerraSAR-X, the negative VTEC percent is pretty large. This might be associated with the poorer quality of code observations and the A/DLECT around the sunrise/sunset time which leads to the stronger horizontal gradients of electron density (see Sect. 3.5). The negative VTEC percentage exhibits similar results for the LEO satellites with the same altitude and the identical space-borne receiver (e.g., Swarm, Sentinel satellites).

The negative VTEC percentages of Sentinel-1A and Sentinel-1B satellites for all multi-LEO solutions are displayed in Fig. 13. With increasing number of LEO satellites, the negative VTEC percentage gets reduced gradually for both Sentinel-1A and Sentinel-1B satellites. When the LEO number reaches nine, the percentage drops from 30.4% and 22.1% to 17.1% for Sentinel-1A and Sentinel-1B satellite, respectively. It is worth noting that the negative VTEC percentage gets slightly larger with the inclusion of MetOp satellites, which is consistent with the stability results of GPS satellite DCB. The results indicate that the VTEC estimation can benefit from the increase in LEO satellites in reducing the percentage of negative VTEC estimates. This benefit can be attributed to the fact that the inclusion of more LEO satellites brings about more available observations, which can improve the strength of the VTEC estimation and achieve more reliable VTEC estimation results. We note that despite the improvement of VTEC results, the percentage of negative VTECs is still beyond 25% and

Fig. 12 Negative VTEC percentage of each LEO satellite for all single-LEO solutions

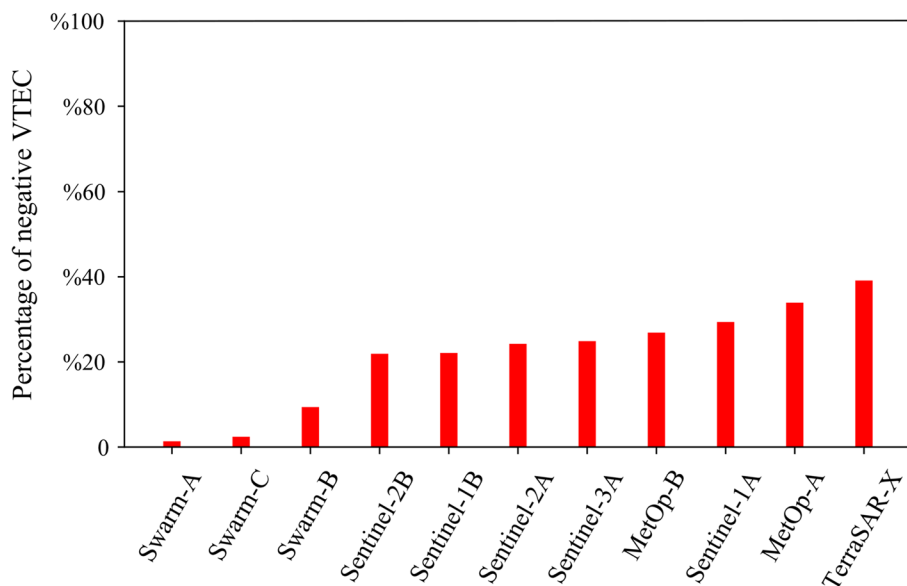
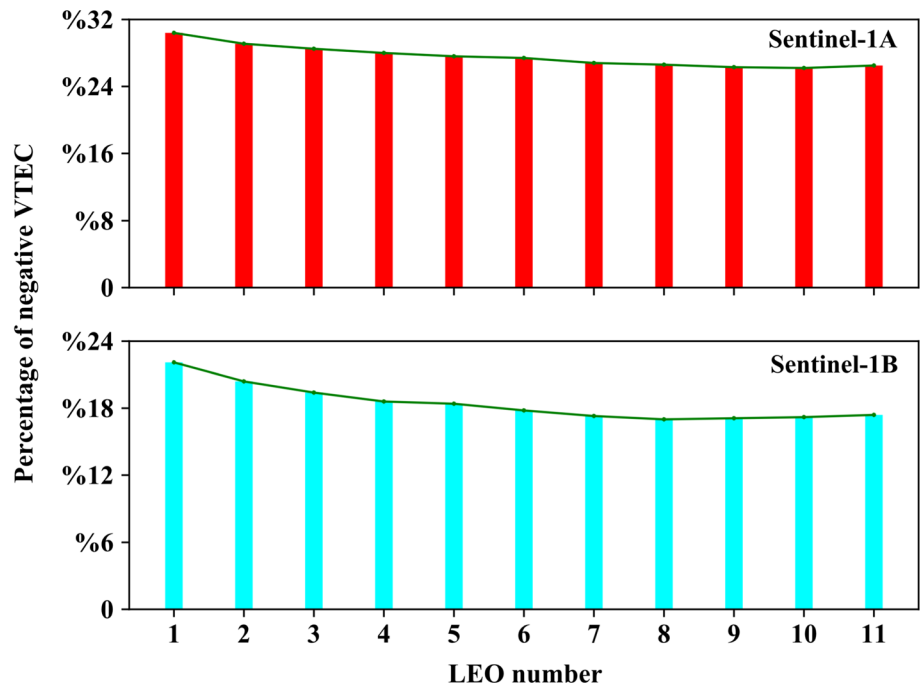


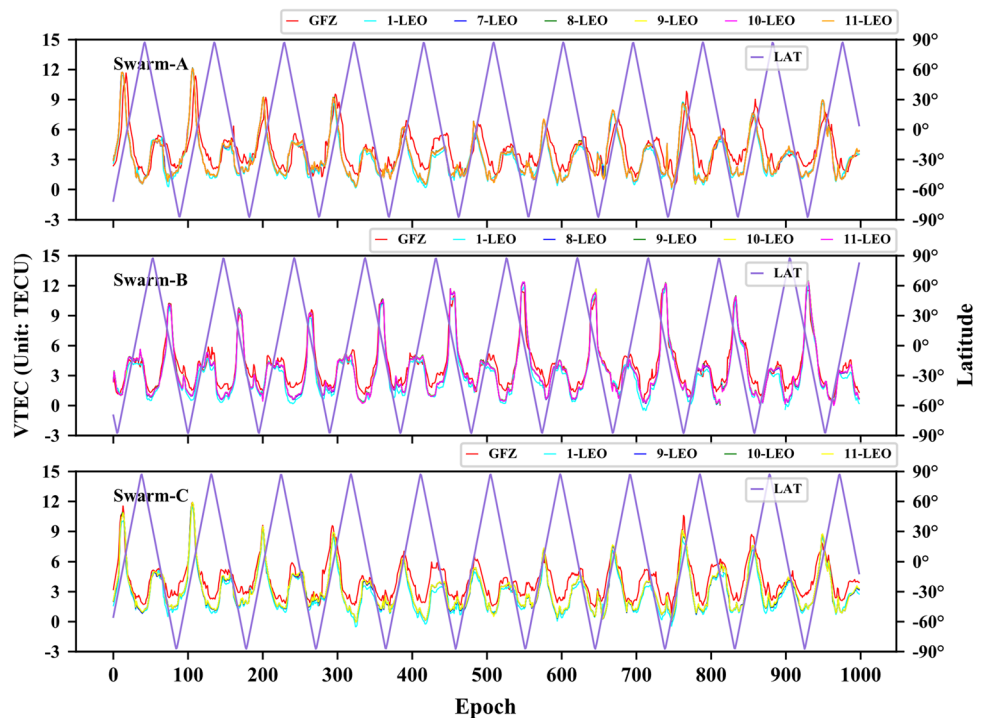
Fig. 13 Percentage of negative VTEC estimates of Sentinel-1A and Sentinel-1B satellites for all multi-LEO solutions. The green line shows the percentage variation trend for all solutions



15% for Sentinel-1A and Sentinel-1B, respectively. Due to the low electron density of the topside ionosphere above the LEO satellite at high altitude, the estimated VTEC can easily become negative even though the DCB estimation is with small uncertainty. The remaining negative VTECs, therefore, might be mainly associated with this cause. In addition, the application of the spherical symmetry assumption might also partly lead to the negative VTEC, which

will be discussed in Sect. 3.5. We have also compared our VTEC estimates of Swarm satellites and the VTEC products released by GFZ as shown in Fig. 14. The results indicate that our estimated VTEC of Swarm satellites agree well with the VTEC products. In addition, the inclusion of more LEO observations can bring about the raise of VTEC values and makes the estimated VTEC closer to the VTEC products. Since the LEO-based VTEC estimation is of great value to

Fig. 14 VTEC of Swarm-A, Swarm-B and Swarm-C for different solutions. The red line represents the VTEC products of Swarm satellites released by GFZ



study the ionosphere, especially in investigating the topside ionosphere and plasmasphere (Lee et al. 2013; Zhong et al. 2017), the further investigation can help us understand the physical mechanisms of topside ionosphere better.

3.5 Analysis of posterior residuals

Yue et al. (2010) reported that the ionosphere can exhibit a sharp variation at low latitudes. In this situation, the use of spherical symmetry ionosphere assumption might cause accuracy degradation in the DCB estimation. To assess the potential impact of the spherical symmetry ionosphere assumption on the DCB estimation, the posterior residuals of each LEO satellite are analyzed in this part.

The posterior residuals of geometry-free observations with respect to the local time (LT) on DOY 120 of 2018 for all LEO satellites are displayed in Fig. 15. The residuals are distributed mainly around two certain LTs. For sun-synchronous orbiting satellites, there two LTs are exactly the A/DLECT (see Table 1). As the orbits of these LEO satellites are near polar, most residuals cluster at the LT of ascending and descending node. This can cause an apparent wider spread of the residuals around A/DLECT, which can explain the residual distribution. The similar residual performance can be found for Swarm satellites despite the drifting orbits. This is mainly because the LECT of Swarm satellites changes slowly, so it exhibits little variation in one day. For MetOp-A/B and TerraSAR-X satellites, the residuals exhibit larger amplitude, which can be

attributed to the poorer quality of code observations (see Fig. 3). By comparison, TerraSAR-X satellite exhibits the largest residuals around A/DLECT. Considering the A/DLECT of TerraSAR-X is around the sunset/sunrise time (see Table 1) when the ionosphere exhibits a sharp variation, the largest residuals might also be associated with the stronger horizontal gradients of electron density.

To further investigate the potential impact of the spherical symmetry ionosphere assumption on the DCB estimation, we have also drawn the posterior residuals of geometry-free observations with respect to the latitudes from DOY 061 to DOY 120 of 2018 for all LEO satellites as displayed in Fig. 16. The residuals show a variation ranging from -3 TECU to 3 TECU for most LEO satellites except for MetOp-A/B and TerraSAR-X satellites which exhibit larger amplitude. There are generally two peaks around 30°S and 30°N for some LEO satellites such as MetOp-A/B, Swarm-A/C, and TerraSAR-X. Two small, but still visible peaks can also be found in the residuals of other LEO satellites such as Sentinel-1A/1B/2A/2B/3A and Swarm-B. This agrees well with the results reported by Yue et al. (2010). Considering the strong horizontal gradients of electron density at low latitudes, the VTECs for all observed GPS satellites at a given epoch can differ a lot. Thus, the spherical symmetry assumption might not be satisfied. The residual peaks can be attributed to the accuracy degradation caused by the spherical symmetry assumption at low latitudes.

Fig. 15 Posterior residuals with respect to the local time on DOY 120 of 2018 for all LEO satellites

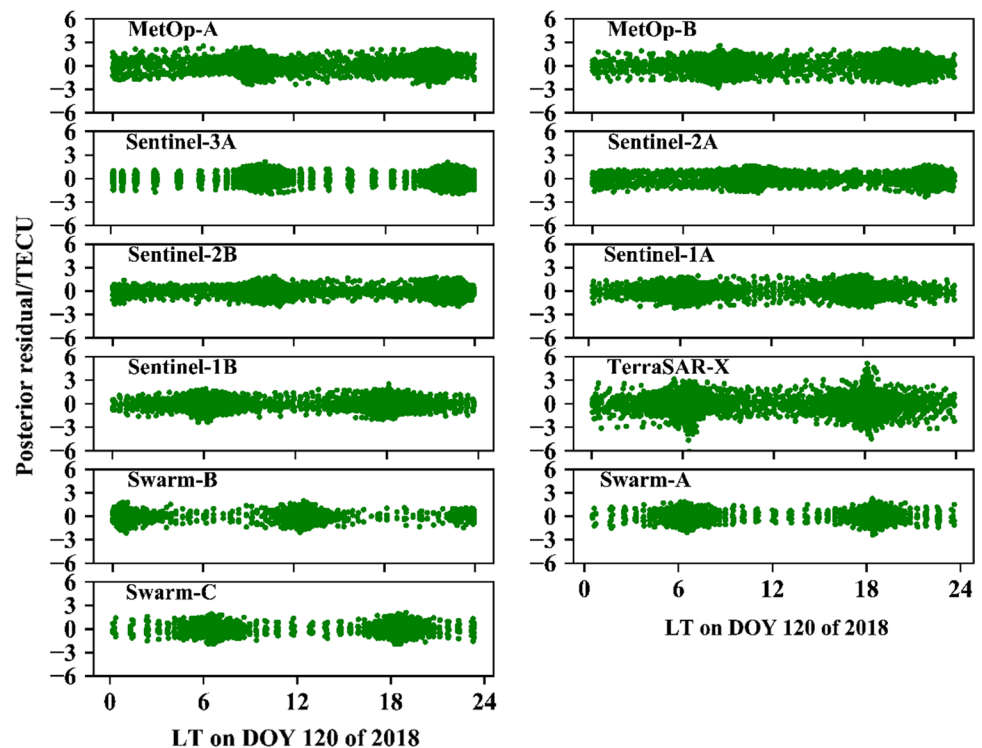
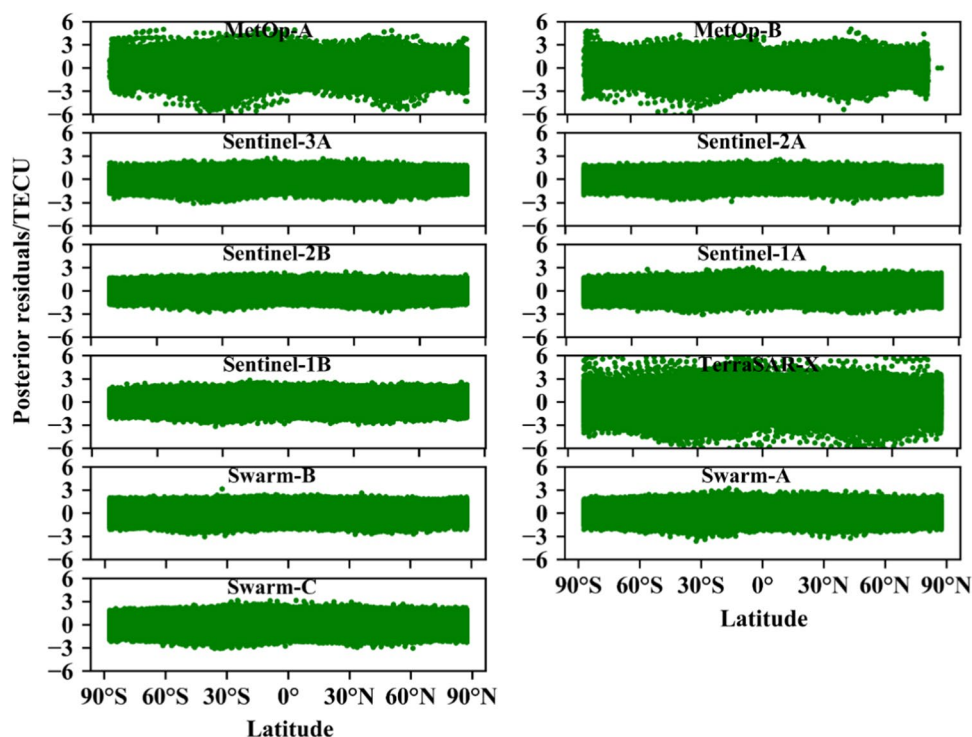


Fig. 16 Posterior residuals with respect to the latitudes from DOY 061 to DOY 120 of 2018 for all LEO satellites



3.6 Discussion

Since the DCB is of vital significance in precise GNSS applications, the determination of DCB has been investigated by numerous researchers based on the ground station observations or onboard observations from single LEO satellite. Considering the available observations from lots of LEO satellites, we have described the multi-LEO based method in the DCB estimation and performed the DCB estimation using observations from currently eleven LEO satellites to investigate the contribution of multi-LEO combination to the DCB estimation in this paper. Our results suggest that the GPS DCB estimated by observations from nine LEO satellites can be comparable to that based on hundreds of ground stations. Moreover, the LEO space-borne receiver DCB and the VTECs can also gain accuracy improvement from the multi-LEO combination. In addition, we also analyzed the multipath errors of code observations and discussed the suitability of spherical symmetry assumption from the view of the posterior residuals. Some drawbacks, however, are also exposed in the LEO-based DCB estimation, such as the generation of negative VTECs.

It is generally recognized that the LEO onboard observations have the advantages of high vertical resolution and global distribution compared to the ground-based observations (Yue et al. 2011). Besides, the observations from LEO satellites can be less affected by the ionosphere ionization owing to the higher altitude which is usually higher than the ionosphere peak height. Nevertheless, the VTEC can be

much smaller in the DCB estimation using LEO observations than those estimated by ground observations due to the high orbit altitude, which can, therefore, become negative easily when the estimation strength is weak. To improve the estimation strength, the quality control of observations and the refinement of parameter configuration are required (Zhong et al. 2016c). Different from the ground stations, due to the quick movement of the LEO satellite, the environment temperature changes sharply which can significantly influence the space-borne receiver. The assumption of the constant receiver DCB during one day, therefore, might be challenged (Yuan et al. 2020). This might be another drawback in the LEO-based DCB estimation. For ground stations, the multipath errors can usually be minimized by discarding low elevation observations (Yue et al. 2011). The multipath errors of LEO onboard observations are worse-than-expected, which makes the method used for the ground stations not applicable. Hence, the multipath errors of LEO onboard observations have to be corrected before the DCB estimation as discussed in Sect. 3.1. Our results also reveal that the spherical symmetry assumption might cause accuracy degradation in the LEO-based DCB estimation at low latitudes.

The geometry-free model which smooths pseudorange by carrier phase is commonly adopted in the LEO-based DCB estimation. The application of the geometry-free model in the LEO-based DCB estimation, however, might weaken the benefit of fast motion of LEO satellites. Thanks to the modification of processing models in the precise orbit

determination of LEO satellites, such as the refinement of the nonconservative force model, the calibration of LEO receiver PCV, and the application of the ambiguity-fixed carrier phase observations, the orbit accuracy of LEO satellites has been improved significantly and can reach sub-centimeter (Hackel et al. 2016; Montenbruck et al. 2018; Kang et al. 2020). The uncombined PPP model, therefore, can be introduced in the LEO-based DCB estimation and exhibits promising performance owing to the improved orbit accuracy (Zhou et al. 2020). In terms of the collection of observations, the access of LEO onboard data is more difficult than that of ground-based observations, particularly for the real-time data currently, which hampers the real-time LEO-based DCB estimation. But this problem can be solved with the launch of communication and navigation LEO constellation missions, such as LeoSat and Hongyan in the near future (Reid et al. 2016; Li et al. 2019b). The high-speed broadband internet services of those LEO constellation will make it possible to collect the onboard observations with low latency, even in real time. In that case, more contribution of LEO onboard observations to the DCB estimation can be expected. In summary, the DCB estimation using LEO onboard data outperforms the ground-based DCB estimation in some aspects and proves to be an effective alternative of the DCB estimation. The drawbacks in the LEO-based method still exist and need further investigation.

4 Summary and conclusions

This study has investigated the contribution of multi-LEO combination to the DCB estimation. Eleven LEO satellites at different altitudes were selected, and the corresponding onboard observations during the period from DOY 061, 2018 to DOY 120, 2018 have been utilized to estimate the GPS P2-C1 DCB. We have designed different single-LEO solutions and multi-LEO solutions to study the influence of LEO satellite number on the DCB estimation. To remove the negative impact of code multipath errors on the DCB estimation, the multipath errors of each LEO satellite have been corrected before the estimation.

The DCB estimation results based on observations from single LEO satellite were firstly evaluated. The average STD values of GPS DCBs are within 0.22 ns for all single-LEO solutions. The best stability is achieved by Swarm-B solution with a STD value of 0.082 ns. Similar performance in GPS DCB stability can be observed for the LEO satellites with identical space-borne receiver. Our estimation results of LEO onboard receiver DCB also agree well with the external DCB products.

For multi-LEO solutions, the GPS DCB stability improves gradually with increasing number of LEO satellites. The 9-LEO solution can achieve the stability with an

average STD value of 0.051 ns, which is slightly better than that of DLR but slightly worse than the result of CAS. Our results reveal that the GPS DCB stability based on the LEO onboard observations from nine LEO satellites can offer stability comparable to the ground-based solution derived from a global ground network with hundreds of stations. The estimated DCBs of most GPS satellites exhibit a difference within 0.5 ns w.r.t. DLR/CAS products, which also benefit from the increase in LEO satellites in improving the consistency between our results and DLR/CAS products. For the receiver DCB results, we find that the multi-LEO combination can contribute to the stability improvement of LEO onboard receiver DCB.

The VTEC estimation results are also assessed. Our VTEC results are in good agreement with the external VTEC products. In addition, the negative VTEC percentage gets reduced gradually as the number of LEO satellites increases, implying that the VTEC estimation can also benefit from multi-LEO combination in reducing the percentage of negative VTEC estimates. The posterior residuals reveal that the application of spherical symmetry ionosphere assumption might cause accuracy degradation in the DCB estimation at low latitudes.

In this study, we have demonstrated the great potential of multi-LEO combination in the DCB estimation. It turns out that the GPS DCB estimation based on the onboard observations from several LEO satellites can reach the precision of DCB products estimated by hundreds of ground stations in terms of the DCB stability. In comparison with the ground-based DCB solution, the LEO-based DCB solution has some significant advantages, such as the high vertical resolution and global distribution. The drawbacks in the LEO-based method, such as the negative VTECs, however, still exist and need further investigation. With the launch of numerous LEO satellites equipped with space-borne multi-GNSS receivers and the modification of the DCB estimation method in the near future, more contribution of LEO onboard observations to the multi-GNSS DCB estimation can be expected. Furthermore, LEO satellites can also benefit from the high-precision multi-GNSS DCBs in POD and fulfill the scientific goals more effectively. Additionally, the onboard multi-GNSS observations from plenty of LEO satellites can be utilized to study the topside ionosphere and contribute a lot to revealing the relationship between the ionosphere and the space events.

Acknowledgements The authors would like to thank ESA, COSMIC Data Analysis and Archive Center (CDAAC) and IGS for providing the free LEO onboard data and the GNSS satellite orbits. Thanks also go to the DLR and the CAS for providing the DCB products. This work has been supported by the National Natural Science Foundation of China under Grant 41774030, Grant 41974027, and Grant 41974029, in part by the Hubei Province Natural Science Foundation of China under Grant 2018CFA081. The numerical calculations have been done on

the supercomputing system in the Supercomputing Center of Wuhan University (<http://hpc.whu.edu.cn/>).

Author contributions X. Li, W. Zhang, and K. Zhang designed the research; X. Li and W. Zhang performed the research; X. Li, W. Zhang and K. Zhang wrote the paper; W. Zhang and K. Zhang analyzed the data; Q. Zhang contributed to the paper writing and the data analyzes; X. Li and Z. Jiang provided valuable help during the revision of the paper; Q. Zhang, X. Ren, X. Li, and Y. Yuan gave helpful suggestions during the internal reviewing process.

Data availability The LEO satellite onboard GNSS observation data are available publicly from GFZ (ftp://swarm-diss.eo.esa.int/Level1b/Latest_baselines/GPSx_RO_ESA) (<https://scihub.copernicus.eu/dhus/#/home>) and CDAAC (<https://cdaac-www.cosmic.ucar.edu/cdaac/rest/tarservice/data>). The broadcast ephemeris data of GNSS satellites are from IGS (<ftp://cddis.gsfc.nasa.gov/pub/gps/data/campaign/mgex/daily/rinex3>; <ftp://cddis.gsfc.nasa.gov/pub/gps/data/daily>). The DCB products can be downloaded publicly from CAS (<ftp://ftp.gipp.org.cn/project/dcb/mgexdcb/>), DLR (<ftp://cddis.gsfc.nasa.gov/pub/gps/products/mgex/dcb/>) and GFZ (ftp://swarm-diss.eo.esa.int/Level2daily/Latest_baselines/TEC). Main results assessed in this manuscript can be accessed from <http://igmas.users.sgg.whu.edu.cn/group/tool/9>.

References

- Aschbacher J, Milagro-Pérez MP (2012) The European Earth monitoring (GMES) programme: status and perspectives. *Remote Sens Environ* 120:3–8
- Bankey V, Anveshkumar N (2015) Design and performance issues of Microstrip antennas. *Int J Sci Eng Res* 6(3):1572–1580
- Blewitt G (1990) An automatic editing algorithm for GPS data. *Geophys Res Lett* 17(3):199–202
- Edwards PG, Berruti B, Blythe P, Callies J, Carlier S, Fransen C, Krusch R, Lefebvre A-R, Loiselet M, Stricker N (2006) The MetOp satellite—weather information from polar orbit. *ESA Bull* 127(127):8–17
- Feltens J (2003) The activities of the ionosphere working group of the International GPS Service (IGS). *GPS Solut* 7(1):41–46
- Foelsche U, Kirchengast G (2002) A simple “geometric” mapping function for the hydrostatic delay at radio frequencies and assessment of its performance. *Geophys Res Lett* 29(10):1473
- Friis-Christensen E, Lühr H, Knudsen D, Haagmans R (2008) Swarm—an Earth observation mission investigating geospace. *Adv Space Res* 41(1):210–216
- Gao S, Clark K, Unwin M, Zackrisson J, Shiroma WA, Akagi JM, Maynard K, Garner P, Boccia L, Amendola G, Massa G, Underwood C, Brenchley M, Pointer M, Sweeting MN (2009) Antennas for modern small satellites. *IEEE Antennas Propag Mag* 51(4):40–56
- Ge Y, Zhou F, Sun B, Wang S, Shi B (2017) The impact of satellite time group delay and inter-frequency differential code bias corrections on multi-GNSS combined positioning. *Sensors* 17:602
- Hackel S, Montenbruck O, Steigenberger P, Balss U, Gisinger C, Eineder M (2016) Model improvements and validation of terrasar-x precise orbit determination. *J Geod* 91:547–562
- Heise S, Jakowski N, Wehrenpennig A, Reigber Ch, Lühr H (2002) Sounding of the topside ionosphere/plasmasphere based on GPS measurements from CHAMP: initial results. *Geophys Res Lett* 29:14
- Hernández-Pajares M, Juan J, Sanz J (1999) New approaches in global ionospheric determination using ground GPS data. *J Atmos Sol Terr Phys* 61(16):1237–1247
- Hernández-Pajares M, Juan J, Sanz J, Arasgón-Àngel À, García-Rigo A, Salazar D, Escudero M (2011) The ionosphere: effects, GPS modeling and the benefits for space geodetic techniques. *J Geod* 85:887–907
- Hernández-Pajares M, Juan J, Sanz J, Orus R, Garcia-Rigo A, Feltens J, Komjathy A, Schaer S, Krankowski A (2009) The IGS VTEC maps: a reliable source of ionospheric information since 1998. *J Geod* 83(3):263–275
- Hwang C, Tseng TP, Lin TJ, Svehla D, Hugentobler U, Chao BF (2010) Quality assessment of FORMOSAT-3/COSMIC and GRACE GPS observables: analysis of multipath, ionospheric delay and phase residual in orbit determination. *GPS Solut* 14(1):121–131
- Jäggi A, Dach R, Montenbruck O, Hugentobler U, Bock H, Beutler G (2009) Phase center modeling for LEO GPS receiver antennas and its impact on precise orbit determination. *J Geod* 83(12):1145–1162
- Kang Z, Bettadpur S, Nagel P, Save H, Poole S, Pie N (2020) GRACE-FO precise orbit determination and gravity recovery. *J Geod* 94:85
- Lee HB, Jee G, Kim YH, Shim JS (2013) Characteristics of global plasmaspheric TEC in comparison with the ionosphere simultaneously observed by Jason-1 satellite. *J Geophys Res Space Phys* 118:935–946
- Li H, Li B, Lou L, Yang L, Wang J (2016) Impact of GPS differential code bias in dual- and triple-frequency positioning and satellite clock estimation. *GPS Solut* 21:897–903
- Li W, Li M, Shi C, Fang R, Zhao Q, Meng X, Yang G, Bai W (2017) GPS and BeiDou differential code bias estimation using Fengyun-3C satellite onboard GNSS observations. *Remote Sens* 9(12):1239
- Li X, Li X, Yuan Y, Zhang K, Zhang X, Wickert J (2018a) Multi-GNSS phase delay estimation and PPP ambiguity resolution: GPS, BDS, GLONASS. *Galileo J Geod* 92(6):579–608
- Li X, Xie W, Huang J, Ma T, Zhang X, Yuan Y (2018b) Estimation and analysis of differential code biases for BDS3/BDS2 using iGMAS and MGEX observations. *J Geod* 93(3):419–435
- Li X, Ma T, Xie W, Zhang K, Huang J, Ren X (2019a) FY-3D and FY-3C onboard observations for differential code biases estimation. *GPS Solut* 23:57
- Li X, Ma F, Li X, Lv H, Bian L, Jiang Z, Zhang X (2019b) LEO constellation-augmented multi-GNSS for rapid PPP convergence. *J Geod* 93(5):749–764
- Li Z, Yuan Y, Fan L, Huo X, Hsu H (2014) Determination of the differential code bias for current BDS satellites. *IEEE Trans Geosci Remote Sens* 52(7):3968–3979
- Lin J, Yue X, Zhao S (2014) Estimation and analysis of GPS satellite DCB based on LEO observations. *GPS Solut* 20(2):251–258
- Liu M, Yuan Y, Huo X, Li M, Chai Y (2020) Simultaneous estimation of GPS P1–P2 differential code biases using low earth orbit satellites data from two different orbit heights. *J Geod* 94(12):121
- Mannucci AJ, Wilson BD, Yuan DN, Ho CH, Lindqwister UJ, Runge TF (1998) A global mapping technique for GPS-derived ionospheric total electron content measurements. *Radio Sci* 33(3):565–582
- Montenbruck O, Kroes R (2003) In-flight performance analysis of the CHAMP BlackJack GPS receiver. *GPS Solut* 7(2):74–86
- Montenbruck O, Andres Y, Bock H, Helleputte T, Ijssel J, Loiselet M, Marquardt C, Silvestrin P, Visser P, Yoon Y (2008) Tracking and orbit determination performance of the GRAS instrument on MetOp-A. *GPS Solut* 12:289–299
- Montenbruck O, Garcia-Fernandez M, Yoon Y, Schon S, Jäggi A (2009) Antenna phase center calibration for precise positioning of LEO satellites. *GPS Solut* 13(1):23–34
- Montenbruck O, Hauschild A, Steigenberger P (2014) Differential code bias estimation using multi-GNSS observations and global ionosphere maps. *Navigation* 61(3):191–201

- Montenbruck O, Hackel S, Jaggi A (2018) Precise orbit determination of the Sentinel-3A altimetry satellite using ambiguity-fixed GPS carrier phase observations. *J Geod* 92:711–726
- Öhgren M, Bonnedal M, Ingvarson P (2011) GNSS antenna for precise orbit determination including S/C interference predictions. In: European conference on antennas & propagation. IEEE
- Noja M, Stolle C, Park J, Lühr H (2013) Long-term analysis of ionospheric polar patches based on champ tec data. *Radio Sci* 48(3):289–301
- Reid TGR, Neish AM, Walter TF, Enge PK (2016) Leveraging commercial broadband LEO constellations for navigation. In: Proceedings of the 29th international technical meeting of the satellite division of the institute of navigation (ION GNSS+2016), Portland, Oregon, September 2016, pp 2300–2314
- Sanz J, Juan JM, Rovira-Garcia A, González-Casado G (2017) GPS differential code biases determination: methodology and analysis. *GPS Solut* 21(4):1549–1561
- Schaer S (1999) Mapping and predicting the earth's ionosphere using the global positioning system. *Geod. -Geophys. Arb. Schweiz* 59(59)
- Tapley BD, Bettadpur S, Watkins M, Reigber C (2004) The gravity recovery and climate experiment: mission overview and early results. *Geophys Res Lett* 31(9):L09607
- Wang N, Yuan Y, Li Z, Montenbruck O, Tan B (2015) Determination of differential code biases with multi-gnss observations. *J Geod* 90(3):209–228
- Wautelet G, Loyer S, Mercier F, Perosanz F (2017) Computation of GPS P1–P2 differential code biases with Jason-2. *GPS Solut* 21(4):1619–1631
- Yuan L, Jin S, Hoque M (2020) Estimation of LEO-GPS receiver differential code bias based on inequality constrained least square and multi-layer mapping function. *GPS Solut* 24:57
- Yue X, Schreiner WS, Lei J, Sokolovskiy SV, Rocken C, Hunt DC, Kuo YH (2010) Error analysis of Abel retrieved electron density profiles from radio occultation measurements. *Ann Geophys* 28:217–222
- Yue X, Schreiner WS, Hunt DC, Rocken C, Kuo YH (2011) Quantitative evaluation of the low earth orbit satellite based slant total electron content determination. *Space Weather* 9(9):S09001
- Zakharenkova I, Cherniak I (2015) How can GOCE and TerraSAR-X contribute to the topside ionosphere and plasmasphere research? *Space Weather* 13(5):271–285
- Zhang X, Tang L (2014) Daily global plasmaspheric maps derived from COSMIC GPS observations. *IEEE Trans Geosci Remote Sens* 52(10):6040–6046
- Zhong J, Lei J, Dou X, Yue X (2016a) Is the long-term variation of the estimated GPS differential code biases associated with ionospheric variability? *GPS Solut* 20(3):313–319
- Zhong J, Lei J, Dou X, Yue X (2016b) Assessment of vertical TEC mapping functions for space-based GNSS observations. *GPS Solut* 20(3):353–362
- Zhong J, Lei J, Dou X, Yue X (2016c) Determination of differential code bias of GNSS receiver onboard low earth orbit satellite. *IEEE Trans Geosci Remote Sens* 54(8):4896–4905
- Zhong J, Lei J, Wang W, Burns AG, Yue X, Dou X (2017) Longitudinal variations of topside ionospheric and plasmaspheric TEC. *J Geophys Res Space Phys* 122:6737–6760
- Zhou P, Nie Z, Xiang Y, Wang J, Du L, Gao Y (2020) Differential code bias estimation based on uncombined PPP with LEO onboard GPS observations. *Adv Space Res* 65(1):541–551